J Geod (2005) 79: 160–166
DOI 10.1007/s00190-005-0455-0

ORIGINAL ARTICLE

P.N.A.M. Visser

Low-low satellite-to-satellite tracking: a comparison between analytical linear orbit perturbation theory and numerical integration

Received: 22 January 2004 / Accepted: 17 March 2005 / Published online: 5 May 2005

Abstract Low-low satellite-to-satellite tracking (ll-SST) range-rate observations have been predicted by two methods: one based on a linear perturbation theory in combination with the Hill equations, and one based on solving the equations of motion of two low-flying satellites by numerical integration. The two methods produce almost equivalent Fourier spectra of the range-rate observations after properly taking into account a few resonant terms. For a typical GRACE-type configuration, where the two satellites trail each other at a distance of 300 km at an altitude of 460 km, and in the presence of the EGM96 gravity field model, complete to spherical harmonic degree and order 70, the agreement between the Fourier spectra is about 1 mm/s compared to a root-mean-square (RMS) value of more than 220 mm/s for the range-rate signal. The discrepancy of 1 mm/s can be reduced significantly when not taking into account perturbations caused by the J_2 term. Excluding the J_2 term, the agreement between the two methods improves to 0.4 mm/s compared to a RMS value of 6 mm/s for the range-rate signal. These values are 0.01 and 2.3 mm/s when ignoring the spectrum for frequencies below two cycles per orbital revolution, reducing the discrepancy even further to about 0.5% of the signal. The selected linear perturbation theory is thus capable of modeling gravity field induced range-rate observations with very high precision for a large part of the spectrum.

Keywords Low-low satellite-to-satellite tracking (ll-SST) · Linear perturbation theory (LPT) · Numerical integration (NI)

1 Introduction

The concept of using low-low satellite-to-satellite tracking (ll-SST) for mapping the Earth's global gravity field has been studied for at least over three decades (Wolff 1969). In 2002, this concept was realized with the successful launch of the GRACE satellite pair (Tapley and Reigber 1999; Tapley et al. 2004) in near-polar (89° inclination) near-circular orbits (eccentricity < 0.001) at about 480 km altitude with an inter-satellite distance between 170 km and 270 km. Although many modern precise orbit determination (POD) and gravity field parameter estimation techniques rely on numerical integration techniques (Boyce and DiPrima 1986; Montenbruck and Gill 2000), analytical orbit perturbation theories have proved their value for gravity field satellite mission design studies and performance predictions (Wagner 1983, 1987; Kaula 1983; Visser 1999). Moreover, Colombo (1984) shows that, for certain satellite orbit geometries, a close match can be obtained between ll-SST observations predicted by analytical orbit perturbation theories solving the Hill equations and ll-SST observations that were obtained by solving the equations of motion of a satellite pair by numerical integration.

Cheng (2002) has further refined analytical perturbation theories for ll-SST modeling. He included a detailed description of the observation modeling and analytical perturbation theory, which is partly based on the work of Rosborough (1987). Cheng (2002) shows the high sensitivity of ll-SST observation to high degree and order gravity field coefficients and also indicates the need for high degree and order modeling of tidal perturbations. However, the implementation of the analytical perturbation theory presented in Cheng (2002) was not validated by independent methods, tools or softwares. As will be discussed in this paper, some of the results presented in Cheng (2002) require special attention.

For example, in Sect. 4.1 of Cheng (2002) a large ll-SST range-rate signal of 93 m/s is described with a period of 92 days, and in Sect. 4.1.1 J_2 and J_3 ll-SST signals of 107 and 103 m/s at nearly one and three cycles per orbital revolution (cpr) for a GRACE-type mission, whereas the GRACE ll-SST instrument is designed for a signal magnitude of 1.5 m/s (Gerard Kruizinga, Jet Propulsion Laboratory 2003 Personal communication). These results and discus-

P.N.A.M. Visser
Delft Institute for Earth-Oriented Space Research,
Delft University of Technology,
Kluyverweg 1, 2629 HS, Delft, The Netherlands
Tel.: +31-15-2782595
Fax: +31-15-2785322
E-mail: Pieter.Visser@lr.tudelft.nl

sions partially triggered the research described below. Moreover, in the past, fast and efficient gravity field mission design and performance prediction tools were developed and implemented based on analytical linear perturbation theories (cf. Colombo (1984)). It is expected that the design of future gravity field missions will continue to benefit from these tools.

This paper will first address ll-SST modeling by two independent methods: one based on the linear orbit perturbation theory solution of the Hill equations and one based on numerical integration of the equations of motion of two satellites flying "en echelon" in a low orbit. It will be shown that these two methods provide nearly equivalent results when properly taking into account a few resonant terms. The differences between the two methods cannot account for some of the results described in (Cheng 2002). It will be shown, however, that ll-SST range-rate observations can be modeled to a precision of better than 1% of the total signal, where a large part of the mismatch between the two methods can be attributed to higher-order J_2 effects.

2 Low-low satellite-to-satellite tracking

Typical ll-SST satellite missions for gravity field mapping consist of two satellites that fly at low-altitude (300–500 km) in near co-planar and near-polar circular reference orbits (Wolff 1969). In the sequel, it is therefore assumed that the ll-SST configuration consists of two satellites trailing each other in the same orbital plane.

For the first method, based on a linear orbit perturbation theory, a reference frame is used with the origin in the Earth's center of mass and with the XY-plane coinciding with the nominal orbital plane of the two satellites, herein referred to as the co-planar reference frame. The X axis is aligned with the radius vector of the first satellite according to a nominal circular orbit. The Y axis is perpendicular to the X axis in the nominal orbital plane, aligned with the velocity vector of the circular orbit (Fig. 1). The Z axis is perpendicular to the orbital plane and completes a right-handed orthonormal reference frame.

The distance between the two satellites is defined by the separation angle α, where the second satellite is ahead of the first satellite in the same orbital plane. It is assumed that the orbits of the two satellites are perturbed in the radial (r), transverse (τ), and cross-track (c) directions. These perturbations are denoted by Δr_1, $\Delta\tau_1$ and Δc_1 for the first satellite and Δr_2, $\Delta\tau_2$ and Δc_2 for the second satellite. The inter-satellite range and range-rate satisfy the following equations:

$$\rho = \sqrt{(x_2 - x_1)^2 + (y_2 - y_1)^2 + (z_2 - z_1)^2} \tag{1}$$

$$\rho\dot{\rho} = (\dot{x}_2 - \dot{x}_1) \times (x_2 - x_1) + (\dot{y}_2 - \dot{y}_1) \times (y_2 - y_1) + (\dot{z}_2 - \dot{z}_1) \times (z_2 - z_1), \tag{2}$$

where ρ and $\dot{\rho}$ denote the range and range-rate, respectively, and $x_1, y_1, z_1, x_2, y_2, z_2$ denote the location of the two satellites in the co-planar reference frame. For satellite 1, the coordinates are:

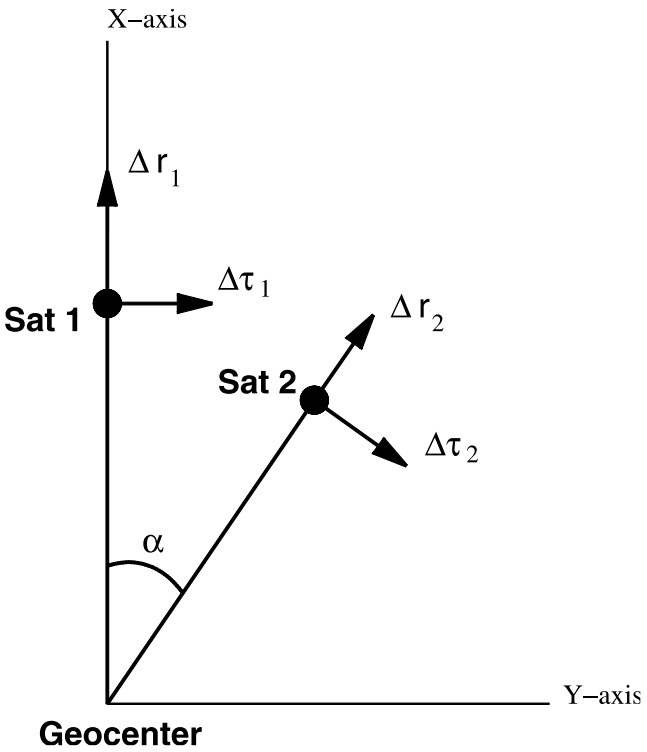

Fig. 1 Configuration of two co-planar satellites and their orbit perturbations

$$x_1 = (r + \Delta r_1) \tag{3}$$

$$y_1 = \Delta\tau_1 \tag{4}$$

$$z_1 = \Delta c_1 \tag{5}$$

and for satellite 2:

$$x_2 = (r + \Delta r_2)\cos\alpha - \Delta\tau_2 \sin\alpha \tag{6}$$

$$y_2 = (r + \Delta r_2)\sin\alpha + \Delta\tau_2 \cos\alpha \tag{7}$$

$$z_2 = \Delta c_2, \tag{8}$$

where r denotes the geocentric radius of the circular reference orbits. Combining Eqs. (2) and (3) to (9) and keeping only the linear terms in Δr, $\Delta\tau$, Δc, $\Delta\dot{r}$, $\Delta\dot{\tau}$, $\Delta\dot{c}$, results in the following relation:

$$\rho\dot{\rho} = r\{(\Delta\dot{r}_2 + \Delta\dot{r}_1)(1 - \cos\alpha) + (\Delta\dot{\tau}_2 - \Delta\dot{\tau}_1)\sin\alpha\} \tag{9}$$

By keeping only the linear terms in the orbit perturbations, the cross-track terms perpendicular to the orbital plane are cancelled in describing the relative motion of the two satellites. For example, the range-rate approximation error $\dot{\rho}_\epsilon$ due to ignoring cross-track orbit perturbations is equal to (using Eqs. (2), (5) and (9)):

$$\dot{\rho}_\epsilon = (\Delta\dot{c}_2 - \Delta\dot{c}_1) \times (\Delta c_2 - \Delta c_1)/\rho. \tag{10}$$

The cross-track velocities $\Delta\dot{c}_1$, $\Delta\dot{c}_2$, are thus multiplied by a factor $(\Delta c_2 - \Delta c_1)/\rho$ compared to $r(1 - \cos\alpha)/\rho$ and $r\sin\alpha/\rho$ for the radial, $\Delta\dot{r}_1$, $\Delta\dot{r}_2$, and along-track velocities, $\Delta\dot{\tau}_1$, $\Delta\dot{\tau}_2$, respectively. Typically, cross-track orbit perturbations are of the same order of magnitude as radial and along-track perturbations (Rosborough 1987) or smaller. In

addition, the cross-track perturbations are at least a few orders of magnitude smaller than the distance between the two satellites (for example 300 km, see Sect. 5). This results in a contribution of the cross-track perturbations to the range-rate observations, which is a few orders of magnitude smaller than the contributions by the radial and along-track terms (cf. Wagner (1987) and Sect. 6 of this paper).

The range according to the nominal circular orbits is equal to:

$$\rho = 2r \sin\frac{\alpha}{2} \tag{11}$$

leading to (after combination with Eq. (9)):

$$\dot\rho \;=\; (\Delta\dot r_2 + \Delta\dot r_1)\sin\frac{\alpha}{2} + (\Delta\dot\tau_2 - \Delta\dot\tau_1)\cos\frac{\alpha}{2}. \tag{12}$$

This range-rate equation (Eq. 12) will be used in conjunction with a linear orbit perturbation theory for predicting gravity-field-induced radial and along-track perturbations for the two satellites.

For the second method, an orthonormal Earth-centered, inertial reference frame (ECI) will be used. The real world is considered to consist of a uniformly rotating Earth with angular rotation rate $\bar\omega$ around the polar $Z_{\rm eci}$ axis. The $X_{\rm eci}$ and $Y_{\rm eci}$ axes are in the equatorial plane, with the $X_{\rm eci}$ axis directing to the Vernal Equinox (true of reference date). The range-rate is obtained by applying the following equations:

$$\begin{aligned}\rho = \big\{&(x_{2,\rm eci} - x_{1,\rm eci})^2 + (y_{2,\rm eci} - y_{1,\rm eci})^2 \\ &+(z_{2,\rm eci} - z_{1,\rm eci})^2\big\}^{\frac{1}{2}}\end{aligned} \tag{13}$$

$$\begin{aligned}\rho\dot\rho = &(\dot x_{2,\rm eci} - \dot x_{1,\rm eci}) \times (x_{2,\rm eci} - x_{1,\rm eci}) \\ &+(\dot y_{2,\rm eci} - \dot y_{1,\rm eci}) \times (y_{2,\rm eci} - y_{1,\rm eci}) \\ &+(\dot z_{2,\rm eci} - \dot z_{1,\rm eci}) \times (z_{2,\rm eci} - y_{1,\rm eci})\end{aligned} \tag{14}$$

where $x_{1,\rm eci}, y_{1,\rm eci}, z_{1,\rm eci}, x_{2,\rm eci}, y_{2,\rm eci}, z_{2,\rm eci}$ denote the location of the two satellites in the ECI reference frame (cf. Eqs. (1) and (2)).

3 Linear perturbation theory

Orbit perturbations in the radial, along-track and cross-track directions caused by spherical harmonic terms of the Earth's gravity field are derived by applying a linear perturbation theory (LPT) assuming circular reference orbits (Kaula 1966; Rosborough 1987). Use is made of the time derivatives of the following equations for the non-resonant terms taken from Visser et al. (2001) (as indicated in Sect. 2, cross-track terms are not taken into account):

$$\begin{aligned}\Delta r = a\sum_{l=2}^{l_{\max}}\sum_{m=0}^{l}\sum_{p=0}^{l}\left(\frac{a_e}{a}\right)^l F_{\rm lmp}\Bigg[&\frac{2(l-2p)}{f_{\rm lmp}} \\ &+\frac{4p-3l-1}{2(f_{\rm lmp}+1)} + \frac{4p-l+1}{2(f_{\rm lmp}-1)}\Bigg] S_{\rm lmp}\end{aligned} \tag{15}$$

$$\begin{aligned}\Delta\tau = a\sum_{l=2}^{l_{\max}}\sum_{m=0}^{l}\sum_{p=0}^{l}\left(\frac{a_e}{a}\right)^l F_{\rm lmp}\Bigg[&\frac{2(l+1)-3(l-2p)\frac{1}{f_{\rm lmp}}}{f_{\rm lmp}} \\ &+\frac{4p-3l-1}{f_{\rm lmp}+1} + \frac{l-4p-1}{f_{\rm lmp}-1}\Bigg] S^*_{\rm lmp}\end{aligned} \tag{16}$$

$$f_{\rm lmp} = l - 2p - m\frac{n_{\rm day}}{n_{\rm rev}} \tag{17}$$

$$\begin{aligned}&S_{\rm lmp}\,(\omega+M, \Omega-\theta) \\ &= \begin{bmatrix}\bar C_{lm}\\ -\bar S_{lm}\end{bmatrix}_{l-m\ \rm odd}^{l-m\ \rm even}\cos((l-2p)(\omega+M)+m(\Omega-\theta)) \\ &\quad+\begin{bmatrix}\bar S_{lm}\\ \bar C_{lm}\end{bmatrix}_{l-m\ \rm odd}^{l-m\ \rm even}\sin((l-2p)(\omega+M)+m(\Omega-\theta))\end{aligned} \tag{18}$$

$$\begin{aligned}&S^*_{\rm lmp}(\omega+M, \Omega-\theta) \\ &= \begin{bmatrix}\bar C_{lm}\\ -\bar S_{lm}\end{bmatrix}_{l-m\ \rm odd}^{l-m\ \rm even}\sin((l-2p)(\omega+M)+m(\Omega-\theta)) \\ &\quad-\begin{bmatrix}\bar S_{lm}\\ \bar C_{lm}\end{bmatrix}_{l-m\ \rm odd}^{l-m\ \rm even}\cos((l-2p)(\omega+M)+m(\Omega-\theta))\end{aligned} \tag{19}$$

where the mean equatorial radius of the Earth is denoted by a_e. Use has been made of the Kepler elements: the orbital semi-major axis a, eccentricity e (only terms of order zero for the eccentricity will be used, assuming near-circular orbits), argument of perigee ω, inclination i, right ascension of ascending node Ω and the mean anomaly M. The Greenwich hour angle is denoted by θ, while $F_{\rm lmp}$ is a normalized function depending on the orbital inclination i only (Chapter 3 in Kaula (1966)). Moreover, it is assumed that the satellite flies in a repeat orbit with a duration of $n_{\rm day}$ nodal days in which $n_{\rm rev}$ orbital revolutions are completed ($n_{\rm day}$ and $n_{\rm rev}$ have to be relative primes for a repeat orbit). The normalized gravity field harmonic coefficients are represented by $\bar S_{lm}$ and $\bar C_{lm}$, where l and m denote the degree and order (for the normalization, see Eq. (1.34) in Kaula (1966)). The gravity field is represented by a spherical harmonic model complete to degree and order $l_{\max}$.

Equations (15)–(19) are almost the same for the two satellites, with the only difference being the value for the argument of latitude:

$$u_1 \;=\; (\omega+M)_1 \tag{20}$$

$$u_2 \;=\; (\omega+M)_1 + \alpha, \tag{21}$$

where u_1 and u_2 denote the argument of latitude of the trailing and leading satellite, respectively. For a repeat orbit, Eqs. (12), (15) to (19), (20) and (21) lead to a Fourier series for the range-rate with basis frequency $1/n_{\rm rev}$ cpr. Resonant terms caused by 0 and 1 cpr gravity-field-induced perturbations have not been included for the moment. These terms occur when $f_{\rm lmp}$ (Eq. (17)) is equal to -1, 0 or +1, which is the case only for zonal terms for the results described in this paper. Resonant terms require special attention, as will be indicated in Sect. 4. For reference, the combination of these

equations lead to an analytical model for ll-SST observations similar to the one described in Wagner (1987).

4 Numerical integration

The ll-SST range-rate observations are also computed based on orbit solutions for the two satellites that are obtained by numerical integration (NI) of the equations of satellite motion. The NI is based on a tenth-order Adams-Moulton integrator (Boyce and DiPrima 1986; Visser et al. 2003) and the orbit solutions are given for each satellite as a series of x, y, z coordinates in the ECI frame with a constant time step. Equations (13) and (14) are then used to obtain a time series of range-rate observations.

Resonant terms are implicitly included when solving the equations of motion by NI. In order to facilitate a direct comparison between range-rates computed by the LPT and by NI, the resonant terms need to be subtracted. As already indicated by Colombo (1984), resonances result in a bow-tie pattern for orbit perturbations. Therefore, in order to enable a comparison with range-rate observations predicted by the LPT, such a bow-tie pattern $\dot{\rho}_{bt}$ will be eliminated from the range-rates using

$$\dot{\rho}_{bt} = a_0 + a_c \cos\omega_{\text{sat}}t + a_s \sin\omega_{\text{sat}}t + b_c\omega_{\text{sat}}t \cos\omega_{\text{sat}}t + b_s\omega_{\text{sat}}t \sin\omega_{\text{sat}}t \quad (22)$$

where ω_{sat} is the satellite's orbital angular velocity and a_0, a_c, a_s, b_s, b_c are constants that are estimated by a least-squares bow-tie fit through the time series of range-rate observations. After subtracting this estimated bow-tie pattern from the range-rate observations, a range-rate amplitude spectrum as a function of frequency (in cpr) will be obtained by a discrete Fourier transform (DFT) .

5 Results

Range-rate observations are simulated for a global gravity field mapping mission with the two satellites flying in a near-circular (eccentricity ≈ 0.001) polar 10-day repeat orbit at 460 km altitude and with a separation of 2.5° ($\approx$ 300 km). The satellites complete 153 orbital revolutions in one repeat period ($n_{\text{day}} = 10$, $n_{\text{rev}} = 153$). A time-series was generated for the period covering September 1–11, 2003. The Earth's gravity field is represented by the EGM96 model complete to spherical harmonic degree and order 70 (Lemoine et al. 1998).

5.1 Linear perturbation theory

The Fourier spectrum for the ll-SST range-rate observations induced by the 70×70 EGM96 model was obtained by directly computing the amplitudes based on Eqs. (15)– (19). It is displayed in Fig. 2 (top left). The root-mean-square (RMS) of the signal, or the root-sum-square (RSS) of the amplitudes divided by $\sqrt{2}$, is equal to 222.4 mm/s. The signal is dominated by a clear 2-cpr peak with an amplitude of 314.4 mm/s (RMS of 222.3 mm/s). Excluding this term leaves an RMS of 6.0 mm/s. Furthermore, relatively large spectral peaks can be observed close to the 1 cpr frequency resonance. It can be observed from Fig. 2 that above 60 cpr, the amplitudes become smaller than 1 μm/s.

5.2 Numerical integration

Fourier spectra were also obtained by the DFT of a time series of ll-SST range-rate observations obtained by NI. The step size in the numerical integration of the equations of motion was taken equal to the observation time interval of 2 s, allowing sufficient data points for the DFT and guaranteeing small numerical integration errors. A total number of 432,000 simulated observations were generated for the selected 10-day period.

As explained in previous Sections, a bow-tie pattern was estimated from the observations first and subtracted before conducting a DFT. The bow-tie pattern has an RMS of 65.3 mm/s. Subtracting this pattern reduced the RMS of the range-rate observations from 232.1 mm/s to 222.8 mm/s, almost equal to the value found in Sect. 5.1. Excluding the 2-cpr term leaves a power of 6.0 mm/s, which is equal to the value found by the prediction based on the LPT. The Fourier spectrum is included in Fig. 2 (top middle) in addition to the differences with respect to the spectrum obtained with the LPT (top right).

6 Comparison and discussion

The power of the ll-SST observations predicted by the LPT and the RMS derived by NI are equal to 222.4 and 222.8 mm/s (after subtracting a bow-tie pattern). The frequency spectrum predicted by the LPT and the Fourier spectrum obtained by a DFT of numerically integrated observations agree very well (top of Fig. 2). The power of amplitude differences is equal to 1.1 mm/s (top right of Fig. 2). The largest amplitude differences occur at frequencies below 5 cpr. Above 15 cpr, all amplitude differences are well below 1 μm/s.

Wagner (1987) indicates that part of the mismatch can be attributed to not taking into account cross-track perturbations. When using Eq. (10) and applying the LPT (Eq. (3) in Visser et al. (2001)) the contribution of periodic terms to the range-rate observations has an RMS value of about 8 μm/s, which explains that only a small part of the mismatch between LPT and NI (cross-track resonant terms might give a bigger contribution, but are for the larger part absorbed by the bow-tie pattern, Eq. (22)).

One has to realize that the Hill equations are a set of linearized equations of motion for perturbations with respect to a circular reference orbit leading to approximation errors (Clohessy and Wiltshire 1960). The results presented in this paper show that these errors lead to a limited range-rate observation error. It is fair to assume that these errors will be reduced

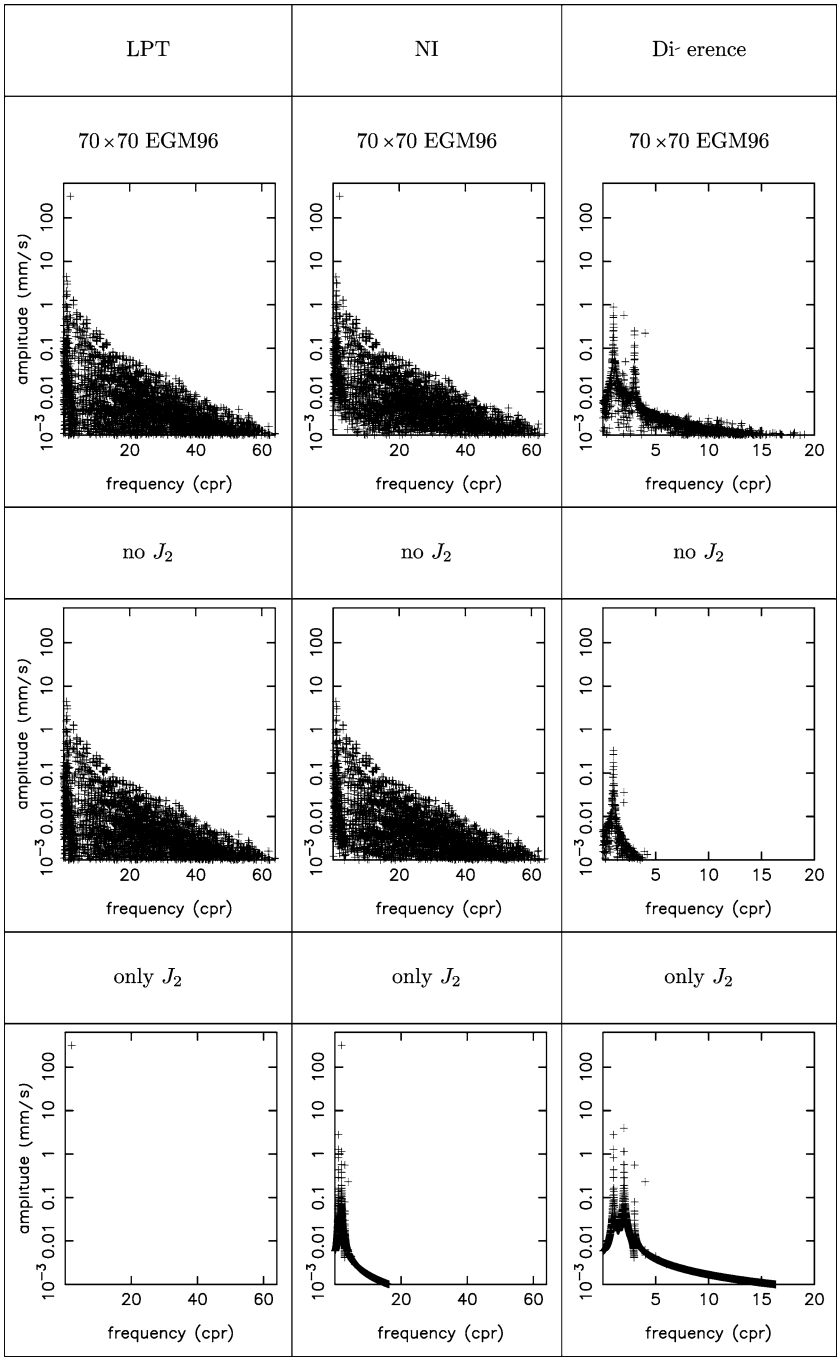

Fig. 2 Spectra of ll-SST observations for two satellite flying "en-echelon" in a 10-day polar repeat orbit at 460 km altitude and separated by 300 km

when the perturbing forces are reduced. The J_2 is the dominant perturbing gravity field term, and it is therefore interesting to assess the range-rate observation error by the LPT when this term is ignored.

Putting the J_2 term equal to zero, the RMS of the range-rate signal becomes 6 mm/s (consistent with the value mentioned in Sect. 5.1 when ignoring the 2-cpr peak). The agreement between the two spectra obtained by the LPT and NI improves from 1.1 mm/s to 0.4 mm/s. These values are 0.01 and 2.3 mm/s when ignoring the spectrum for frequencies below 2 cpr, reducing the discrepancy even further: the LPT modeling error becomes less than 0.5% of the range-rate signal. All amplitude differences are below 1 μm/s above 5 cpr (middle of Fig. 2).

When taking into account only the J_2 term, it was found that the differences between the amplitude spectra obtained by the linear perturbation theory and numerical integration contain most dominant features of the spectra differences when EGM96 is used complete to degree and order 70 (bottom of Fig. 2). Based on these results, it can be concluded

that the largest part of the discrepancy between ll-SST observations predicted by LPT or obtained by NI are due to the J_2 term.

The results presented by Cheng (2002) indicate a much larger power for ll-SST range-rate observations for a similar satellite configuration, with amplitudes up to 93 m/s for a period of 92 days. Amplitudes with this order of magnitude were not found by the two methods described in this paper: the maximum gravity field induced amplitudes are around 30 cm/s. The large amplitudes might be due to the choice of orbit parameters for which perturbation frequencies become almost equal to 0 and 1 (Eq. (17)). For such near-resonant frequencies, the equations for the orbit perturbations might become unstable and fail or lead to unrealistically large amplitudes. Especially when using higher order eccentricity functions in analytical perturbation theories for near-circular orbits, as was done in Cheng (2002), the risk of selecting frequencies very close to 0 and 1 cpr increases, which might result in an overestimation of the size of the orbit perturbation amplitudes. For the results described in Sect. 5.1, only orbit perturbation terms of zero order in the eccentricity were included, where the eccentricity of the orbit used in the numerical integration (Sect. 5.2) was around 0.001.

It might be argued that in Cheng (2002), a gravity field model complete to degree and order 160 was used in the modeling of the range-rate observations, compared to 70 for the computations described so far in this paper. For comparison, the LPT was also applied for a two-month polar repeat orbit ($n_{\text{day}} = 61$, $n_{\text{rev}} = 931$) at approximately the same altitude as Cheng (2002), but using the EGM96 gravity field model complete to degree and order 360. It was found that the RMS of the range-rate signal hardly changed, and – for this case – is equal to 221.5 mm/s, even though through the choice of a two-month repeat period, perturbation frequencies closer to the resonant 0 and 1 cpr appear.

In the case of a change of satellite altitude, a transfer of potential to kinetic energy will take place. A simplified relation has been derived for low-low inter-satellite Doppler or range-rate measurements in Wolff (1969) and in Jekeli (1999):

$$\dot{\rho} \approx \frac{\Delta U}{v}, \tag{23}$$

where v is the velocity of the satellite (taken equal to the nominal circular orbital velocity of the two satellites), and ΔU represents the difference between the gravitational potential at the position of the first and second satellite, respectively. Using the dominant central potential term U_{ct}, the following relation then applies:

$$\dot{\rho} \approx \frac{\Delta U_{ct}}{v} = \frac{\left(\frac{\mu}{r} - \frac{\mu}{r+\Delta h}\right)}{v}, \tag{24}$$

where Δh is the altitude difference between the two trailing satellites. Assuming an altitude of 460 km, an altitude difference between the two satellites of 84 km is required for a velocity difference of 93 m/s. For the simulated 10-day period, the altitude differences were found to range between −300 m and +300 m, which is orders of magnitude smaller and indicative of the much smaller amplitudes for the range-rate observations found in this paper (i.e., 30 cm/s at most). The LPT presented in this paper does not predict ll-SST range-rate signals with amplitudes of the order of 93 m/s, but does produce results that are very close to those obtained by NI (Fig. 2).

As indicated above, the LPT is capable of modeling the range-rate observation with very high precision for the non-dominant components (e.g., J_2) of the gravity field, especially for frequencies above 2 cpr. Equations (12) and (15) to (19) can then possibly be used for estimating gravity field model corrections. Limited gravity field recovery experiments, complete to degree and order 8, were already successfully conducted by Kaula (1983), who made use of an LPT. When extending the estimation of gravity field model coefficients to higher degrees and orders, great care must be taken with near-resonant terms, for example those induced by spherical harmonic orders equal to an integer multiple of the number of revolutions per day. In the notation used in this paper, the number of revolutions per day is equal to $n_{\text{rev}}/n_{\text{day}}$. In Visser et al. (2001), it was found that these near-resonant terms cause gravity field recovery to fail when making use of the LPT and extending the estimation to coefficients with orders larger than $n_{\text{rev}}/n_{\text{day}}$ (or 15 for GRACE-type orbits: thus the maximum order used in Wagner (1983) is much below the first near-resonant order for low-flying satellites).

One has to realize that gravity field estimation from satellite observations is a downward-continuation process, which is inherently unstable (Rummel et al. 1979). This has as a result that, although the LPT is capable of modeling gravity field-induced range-rate observations with high precision, small LPT modeling errors might result in large gravity field recovery errors. However, with the advent of high-precision gravity field models from the GRACE mission (Tapley et al. 2004), the remaining gravity field uncertainty and associated residual range-rate signal is becoming very small, possibly making the LPT capable of efficiently estimating further refinements to these models. This is an interesting topic for further research.

Finally, past experiences have proved that analytical perturbation theories help in designing efficient (preconditioned) iterative gravity field recovery methods, e.g., as described by Klees et al. (2000), Pail and Plank (2002), and Visser et al. (2001, 2003).

7 Conclusions

Relatively simple relations have been derived for co-planar ll-SST observations based on approximated geometric relations and a linear perturbation theory (LPT). These relations were evaluated for a GRACE-type mission scenario to predict ll-SST range-rate frequency spectra in the presence of the 70×70 truncated EGM96 gravity field model. These spectra were validated by spectra obtained by solving the equations of motion through numerical integration (NI). A very

close match was obtained between ll-SST range-rate spectra obtained by LPT and NI after subtracting a bow-tie pattern to account for resonant terms. Remaining discrepancies were found to be mainly caused by higher order J_2 effects. It was found that by ignoring the dominant J_2 term, the LPT range-rate model error is less than 0.5% of the signal for frequencies above 2 cpr. It can thus be argued that the LPT is capable of predicting ll-SST observations induced by gravity field model differences with high precision, for example relative to an accurate a priori gravity field model.

The research described in this paper was partly triggered by Cheng (2002), who presented a detailed analytical perturbation theory for ll-SST modeling and found a few large amplitudes of the order of 100 m/s for ll-SST range-rate observations that cannot be explained by the LPT as formulated in this paper. The results in Cheng (2002) were, however, not validated by an independent method, as is the case here.

The results presented in this paper support earlier work by Colombo (1984) and Wagner (1987), and indicate the suitability of using analytical perturbation theories for gravity field satellite mission design studies and performance predictions. With the advent of accurate high-precision gravity field models from gravity field missions such as GRACE, it is interesting to study whether the LPT described in this paper is suitable for efficiently estimating further refinements to these models.

References

Boyce WE, DiPrima RC (1986) Elementary differential equations and boundary value problems, 4th edn. Wiley, New York

Cheng MK (2002) Gravitational perturbation theory for intersatellite tracking. J Geod. 76(3):169–185

Clohessy WH, Wiltshire RS (1960) Terminal guidance system for satellite rendezvous. J Aerospace Sci 27(9):653–658, 674

Colombo OL (1984) The global mapping of gravity with two satellites, vol 7, no. 3. Netherlands Geodetic Commission, Publications on Geodesy, New Series

Jekeli C (1999) The determination of gravitational potential differences from satellite-to-satellite tracking. Celest Mech Dynam Astronom 75:85–101

Kaula WM (1966) Theory of satellite geodesy. Blaisdell, Waltham

Kaula WM (1983) Inference of variations in the gravity field from satellite-to-satellite range rate. J Geophys Res 88(B10):8345–8349

Klees R, Koop R, Visser P, van den Ijssel J (2000) Efficient gravity field recovery from GOCE gravity gradient observations. J Geod 74(7/8):561–571

Lemoine FG, Kenyon SC, Factor JK, Trimmer RG, Pavlis NK, Chinn DS, Cox CM, Klosko SM, Lutchke SB, Torrence MH, Wang YM, Williamson RG, Pavlis EC, Rapp RH, Olson TR (1998) The development of the joint NASA GSFC and the National Imagery and Mapping Agency (NIMA) Geopotential model EGM96. NASA/TP–1998–206861, Goddard Space Flight Center, Maryland

Montenbruck O, Gill E (2000) Satellite orbits — models methods applications. Springer, Berlin Heidelberg New York, ISBN 3-540-67280-X

Pail R, Plank G (2002) Assessment of three numerical solution strategies for gravity field recovery from GOCE satellite gravity gradiometry implemented on a parallel platform. J Geod 76(8):462–474

Rosborough GW (1987) Radial, transverse, and normal satellite position perturbations due to the geopotential. Celest Mech 40:409–421

Rummel R, Schwarz K, Gerstl M (1979) Least squares collocation and regularization. Bull Géod 53:343–361

Tapley BD, Reigber C (1999) GRACE: a satellite-to-satellite tracking geopotential mapping mission. In: Marson I., Sünkel H., (eds) Bollettino di Geofisica Teorica ed Applicata, vol 40, no. 3–4, Sep.–Dec. 1999, Proceedings of the 2nd joint meeting of the international gravity and the international geoid commission, Trieste 7–12 September 1998, ISSN 0006-6729, p 291

Tapley BD, Bettadpur S, Ries JC, Thompson PF, Watkins MF (2004) GRACE measurements of mass variability in the earth system. Science 305:1503–1505

Visser PNAM (1999) Gravity field determination with GOCE and GRACE. Adv Space Res 23(4):771–776

Visser PNAM, van den Ijssel J, Koop R, Klees R (2001) Exploring gravity field determination from orbit perturbations of the European gravity mission GOCE. J Geod 75(2/3):89–98

Visser PNAM, Sneeuw N, Gerlach C (2003) Energy integral method for gravity field determination from satellite orbit coordinates. J Geod 77(3/4):207–216

Wagner CA (1983) Direct determination of gravitational harmonics from low-low GRAVSAT Data. J Geophys Res 88(B12):10309–10321

Wagner CA (1987) Improved gravitational recovery for a geopotential research mission satellite pair flying en echelon. J Geophys Res 92(B8):8147–8155

Wolff M (1969) Direct measurement of the Earth's gravity potential using a satellite pair. J Geophys Res 74:5295–5300